

Simulation of Cavitating Flows by the Space-Time CE/SE Method

Jian-Rong Qin, S.T. John Yu, Zeng-Chan Zhang, Ming-Chia Lai

Mechanical Engineering Department
Wayne State University

ABSTRACT

The newly developed method of Space-Time Conservation Element and Solution Element, or the CE/SE method for short, is employed to study the complex cavitation phenomenon in this paper. The tenet of the CE/SE method is treating space and time as one entity, and the calculation of flow properties is based on the local and global space-time flux conservation. As a contrast to the modern upwind schemes, no Riemann solver is used, thus the logic of the present scheme for cavitating flows is much simpler. The numerical examples reported in this paper include (1) one-dimensional internal cavitating pipe flows; and (2) two-dimensional external cavitating flows around a NACA0015 airfoil. While we focused on the numerical method in this paper, a simple two-phase homogeneous equilibrium cavitation model was employed in the simulation. We first demonstrated the capability of the CE/SE method to capture contact discontinuities in cavitating fluids, using a hydraulic shock problem. Then we presented the simulation results for cavitating internal pipe flows and external airfoil flows. The numerical results compared favorably with the experimental data and analytical solution.

INTRODUCTION

Cavitation is a very complex two-phase phenomenon. When local flow pressure drops under the vapor pressure of the fluid, bubbles may be formed. The collapse of these bubbles will generate high pressure waves propagating through the pipe, which will lower the performance of the system, produce vibration and noise, and even cause damage to the device surfaces [6]. Numerical simulation of cavitating flows poses unique challenges both in modeling the physics and in developing a robust numerical methodology.

The numerical difficulty of simulating cavitation comes from the fundamental features of the two-phase flow. One of the typical features is the rapid change in the acoustic velocity of the flow. When the void fraction is zero, the fluid is liquid and almost incompressible. Therefore the acoustic velocity is very high. On the other hand, when the void fraction is 1.0, the fluid is vapor and compressible. In between, the acoustic velocity changes remarkably and can be as low as 20m/s [12]. Hence the desired solver must be able to handle compressible and incompressible flows simultaneously. Another feature

that cause numerical instability is the tremendous density difference between gas and liquid. The numerical scheme should be robust enough to deal with these enormous instability problems. Various numerical methods, such as the method of characteristics [8] and high resolution upwind schemes for capturing the interface of two phase flows [11], have been developed to study cavitating flows.

In this paper, we employ a simple homogeneous cavitation model and concentrate on the numerical scheme. We employed the CE/SE method originally developed by Chang [1]. The method is substantially different in both concept and methodology from the traditional methods. It enforces both local and global flux conservation in space-time domain and has remarkable ability to resolve discontinuity interfaces.

The rest of this paper is organized as follows. In Section 2, the essence of the CE/SE method will be illustrated. In Section 3, we discuss the theoretical model of the one-dimensional pipe flows and the simulation results. In Section 4, we present numerical results of two-dimensional cavitating flows around NACA0015 airfoil, using unstructured triangular mesh. We then give the concluding remarks.

3. THE CE/SE METHOD

In this section, we give a brief description of the CE/SE method. For one-dimensional case, the governing equations can be written in the form of

$$\frac{\partial q_m}{\partial t} + \frac{\partial f_m}{\partial x} = s_m(q_1, q_2), \quad (2.1)$$

where m equals 1 and 2, representing the continuity equation and momentum equation, respectively. The source term $s_m(q_1, q_2)$ is a function of q_1 and q_2 . Let $x_1 (= x)$ and $x_2 (= t)$ be the coordinates of a two-dimensional Euclidean space E_2 . Thus Eq. (2.1) becomes

$$\nabla \cdot \mathbf{h}_m = s_m(q_1, q_2) \quad (2.2)$$

in which the current density vector is $\mathbf{h}_m = (f_m, q_m)$. By using Gauss' divergence theorem in the space-time domain E_2 , it can be shown that Eq. (2.1) is the differential form of the integral conservation law:

$$\oint_{S(R)} \mathbf{h}_m \cdot d\bar{s} = \int_R s_m(q_1, q_2) dR \quad (2.3)$$

Figure 1 shows a schematic of Eq. (2.3).

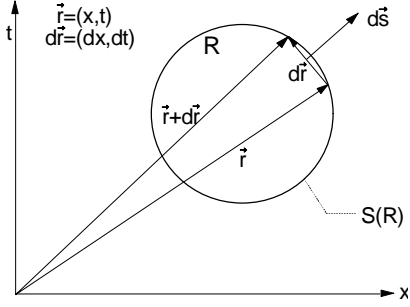


Fig. 1 A schematic of the space-time integral

Here $S(R)$ is the boundary of an arbitrary space-time region R in E_2 , $d\bar{s} = ds\bar{n}$ with ds and \bar{n} , respectively, being the area and the outward unit normal of a surface element on $S(R)$, and dR is the volume of a space-time region inside $S(R)$. Note that $\mathbf{h}_m \cdot d\bar{s}$ is the space-time flux of \mathbf{h}_m leaving the region R through the surface element $d\bar{s}$, and all mathematical operations can be carried out since E_2 is an ordinary two-dimensional Euclidean space. We remark that space and time are treated on an equal footing manner. Therefore, there is no restriction on the space-time geometry of the conservation elements over which the space-time flux is imposed.

In the light of the method of treating stiff source terms proposed by Yu and Chang [13], we discretized the space-time domain into rectangular elements in stead of rhombic ones, and associated the source term with the old time step variables. These treatments enable explicit time marching of this scheme. This is a good approximation since the source term of friction force in the one-dimensional governing equations is not stiff.

3. ONE-DIMENSINAL SIMULATION

3.1 FLOW EQUATIONS

For the compressible liquid flow in a pipe, the governing equations are

$$\frac{\partial \mathbf{Q}}{\partial t} + \frac{\partial \mathbf{E}}{\partial x} = \mathbf{S}. \quad (3.1)$$

The flow variable vector, flux vector, and the source vector are

$$\mathbf{Q} = \begin{pmatrix} \mathbf{r} \\ \mathbf{ru} \end{pmatrix}, \quad \mathbf{E} = \begin{pmatrix} \mathbf{ru} \\ \mathbf{ru}^2 + p \end{pmatrix}, \quad \mathbf{S} = \begin{pmatrix} 0 \\ -\frac{f|u|\mathbf{r}}{2D} \end{pmatrix}, \quad (3.2)$$

in which ρ is density, u is velocity, p is pressure, D is the diameter of the pipe, and f is the Darcy friction factor. In

Eq. (3.1), the first equation is the continuity equation and the second one is the momentum equation. The density and pressure are related by the acoustic velocity a of the liquid, such as

$$\frac{dp}{dr} = a^2. \quad (2.3)$$

The source term in the momentum equation models the viscous friction of fluid flow.

3.3 CAVITATION MODEL

When cavitation occurs, the density in the flow equations is treated as a "psuedo density", which is related to the gas and liquid density by

$$\mathbf{r} = \alpha \mathbf{r}_g + (1-\alpha) \mathbf{r}_l, \quad (3.4)$$

where α is the void fraction. The relation between density, pressure and the speed of sound, Eq. (3.3), needs to be modeled. In this paper a two-phase homogenous equilibrium cavitation model [7] was adopted. The acoustic velocity of the two-phase homogeneous fluid is given by Wallis [12] as

$$a = \left\{ \left[\alpha \mathbf{r}_g + (1-\alpha) \mathbf{r}_l \right] \cdot \left[\frac{\alpha}{\mathbf{r}_g \cdot a_g^2} + \frac{(1-\alpha)}{\mathbf{r}_l \cdot a_l^2} \right] \right\}^{1/2}. \quad (3.5)$$

Substituting Eq. (3.5) into Eq. (3.3) and integrating pressure as a function of void fraction from the saturated liquid state, we have

$$p = p_l^{sat} + p_{gl} \cdot \log \left[\frac{\mathbf{r}_g \cdot a_g^2 \cdot (\mathbf{r}_l + \alpha \cdot (\mathbf{r}_g - \mathbf{r}_l))}{\mathbf{r}_l (\mathbf{r}_g \cdot a_g^2 - \alpha \cdot (\mathbf{r}_g \cdot a_g^2 - \mathbf{r}_l \cdot a_l^2))} \right], \quad (3.6)$$

where p_{gl} is a constant given by

$$p_{gl} = \frac{\mathbf{r}_g \cdot a_g^2 \cdot \mathbf{r}_l \cdot a_l^2 \cdot (\mathbf{r}_g - \mathbf{r}_l)}{\mathbf{r}_g^2 \cdot a_g^2 - \mathbf{r}_l^2 \cdot a_l^2}. \quad (3.7)$$

3.3 SIMULATION RESULTS

Transient hydraulic pressure wave propagation in a pipe is of practical importance in automotive systems, including fuel delivery, power steering, anti-lock brake, engine cooling, and automatic transmission. Many researchers [4, 9, 10] have attempted to simulate the transient wave propagation in the pump-line-nozzle system, which is widely used in diesel engine. But they didn't consider the possible formation of cavitation and its effect on the transient flows. While the maximum pressure generated at the valve can be analytically predicted by neglecting the fluid resistance [3], detailed hydrodynamic simulation can only be achieved by numerical methods.

In this section, two numerical examples are reported. The first problem is a hydraulic shock problem, which demonstrates the capability of the CE/SE method for capturing contact discontinuities. The second problem is the transient waves in a cavitating pipe flow.

3.3.1 Hydraulic Shock Problem

Analytical Solution - Consider an infinitely long tube with a diaphragm located at a certain place. The diaphragm separates two initially quiescent liquid states at different pressures and densities. When the diaphragm is suddenly broken at time $t = 0$, an expansion fan will be formed and propagate to the high-pressure liquid, simultaneously a shock will be formed and propagate to the low-pressure region, as shown in Fig. 2. In this figure, the diaphragm is placed at the lower center and the pressure of the liquid to the left of this diaphragm is higher than that to the right.

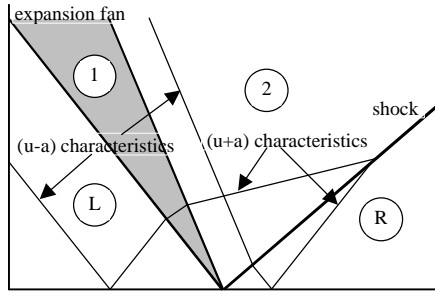


Fig. 2 A description of hydraulic shock problem

In our analysis, we didn't take the source term in Eq. (3.1) into consideration. The initial conditions were set such that no bubble will form during the transient process. With this simplification, Eq. (3.1) can be written as

$$\frac{\partial \mathbf{Q}}{\partial t} + \mathbf{A} \frac{\partial \mathbf{Q}}{\partial x} = 0, \quad (3.8)$$

where \mathbf{A} is the jacobian matrix given by

$$\mathbf{A} = \begin{bmatrix} 0 & 1 \\ a^2 - u^2 & 2u \end{bmatrix}. \quad (3.9)$$

This jacobian matrix \mathbf{A} can be diagonalized by a matrix, say, \mathbf{M} . Multiplying the inverse \mathbf{M}^{-1} to both sides of equation (3.8), we can get the characteristic form

$$\frac{\partial \hat{\mathbf{Q}}}{\partial t} + \Lambda \frac{\partial \hat{\mathbf{Q}}}{\partial x} = 0. \quad (3.10)$$

Where Λ is a diagonal matrix given in Eq. (3.11), and $\hat{\mathbf{Q}}$ is related to \mathbf{Q} by Eq. (3.12).

$$\Lambda = \mathbf{M}^{-1} \mathbf{A} \mathbf{M} = \begin{bmatrix} u+a & 0 \\ 0 & u-a \end{bmatrix} \quad (3.11)$$

$$\frac{\partial \hat{\mathbf{Q}}}{\partial \mathbf{Q}} = \mathbf{M}^{-1} \quad (3.12)$$

By selecting appropriate matrix \mathbf{M} and integrating Eq. (3.12), we have

$$\begin{cases} \hat{q}_1 = u + a \ln r + C_1 \\ \hat{q}_2 = u - a \ln r + C_2 \end{cases}, \quad (3.13)$$

where C_1 and C_2 are two integration constants. Eqs. (3.10) and (3.13) indicate that $u \pm a \ln r$ are two constants along the two characteristics $\frac{dx}{dt} = u \pm a$, respectively. In the expansion fan area, area 1 in Fig. 2, we have

$$\begin{cases} u_1 + a \ln r_1 = u_L + a \ln r_L \\ u_1 - a \ln r_1 = \text{const.} \end{cases} \quad \text{along} \quad \frac{dx}{dt} = u_1 - a. \quad (3.14)$$

From equation (3.14), we know u_1 is a constant along $\frac{dx}{dt} = u_1 - a$. Thus, we get the solution $u_1 = \frac{x - x_0}{t} + a$ in area 1, where x_0 is the initial position of the diaphragm. Density r_1 and other properties can then be obtained using Eq. (3.14). In the area 2 in Fig. 2, we have

$$\begin{cases} u_2 + a \ln r_2 = u_L + a \ln r_L \\ r_2(u_2 - C) = r_R(u_R - C) \\ r_2(u_2 - C)^2 + p_2 = r_R(u_R - C)^2 + p_R \end{cases}, \quad (3.15)$$

where C is the speed of the shock. By assuming constant acoustic velocity a , intergration of Eq. (3.3) gives

$$p = a^2 r + \text{const.} \quad (3.16)$$

Combining Eqs. (3.15) and (3.16) leads to

$$\begin{cases} \frac{r_2 - r_R}{\sqrt{r_2 r_R}} + \ln r_2 = \ln r_L \\ u_2 = \frac{r_2 - r_R}{\sqrt{r_2 r_R}} a \\ C = \frac{r_2 u_2}{r_2 - r_R} \end{cases}. \quad (3.17)$$

This is the exact solution in area 2. The flow properties in area L and R are not changed from their initial value.

Numerical Results - To demonstrate the ability of the CE/SE to capture discontinuity interfaces, we first compute the hydraulic shock problem described above. In this case, our computation domain is from $x = 0\text{m}$ to $x = 1.0\text{m}$. The diaphragm is initially located at $x = 0.5\text{m}$. The initial velocity is 0 everywhere in the tube. The left and right boundaries are set as non-reflect boundaries.

At the bursting of the diaphragm, at time $t = 0$, a rarefaction wave moves to the left and a shock moves to the right.

Figure 3 shows the numerical results plotted against the analytical solutions. In this case, the initial pressure of the liquid (water) to the left of the diaphragm is 2.0MPa and the pressure to the right of the diaphragm 0.1MPa. As shown in Fig. 3, the numerical results agree with the analytical results very well. Two discontinuity steps were successfully captured by the space-time CE/SE scheme. The left step is an expansion fan and the right step is a shock. Since the compressibility of water is very small, the expansion fan looks like a shock.

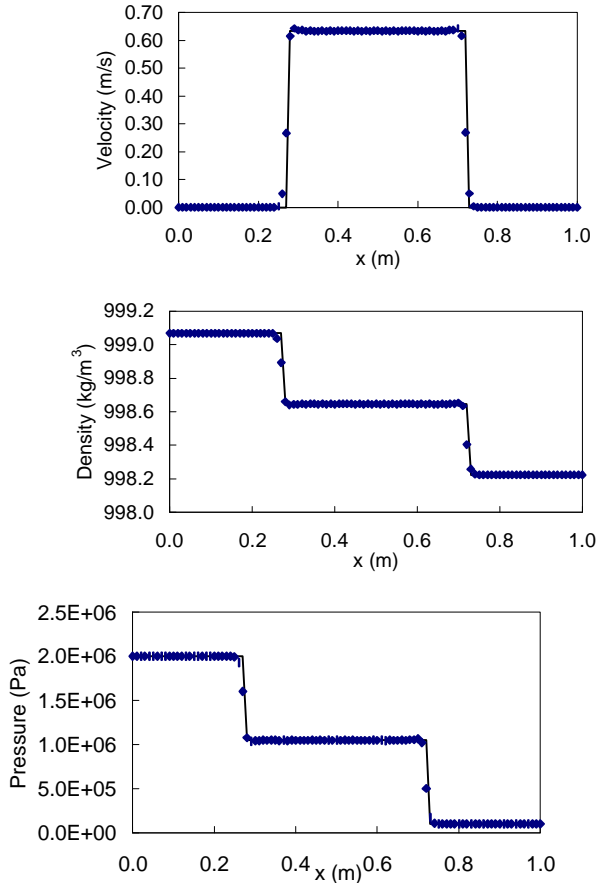


Fig. 3 The CE/SE solution of hydraulic shock problem ($t=0.15 \times 10^{-3}$ sec.)

As the initial pressure difference between the two sides of the diaphragm becomes larger, the expansion fan can be seen more clearly. Shown in Fig. 4 are the numerical and analytical results under the condition of large pressure difference. In this case, the left side pressure is 500MPa, and right side pressure is 1.0MPa. The left side expansion was captured by three points, and the right side shock was captured by one point. The numerical results also agree with analytical results very well.

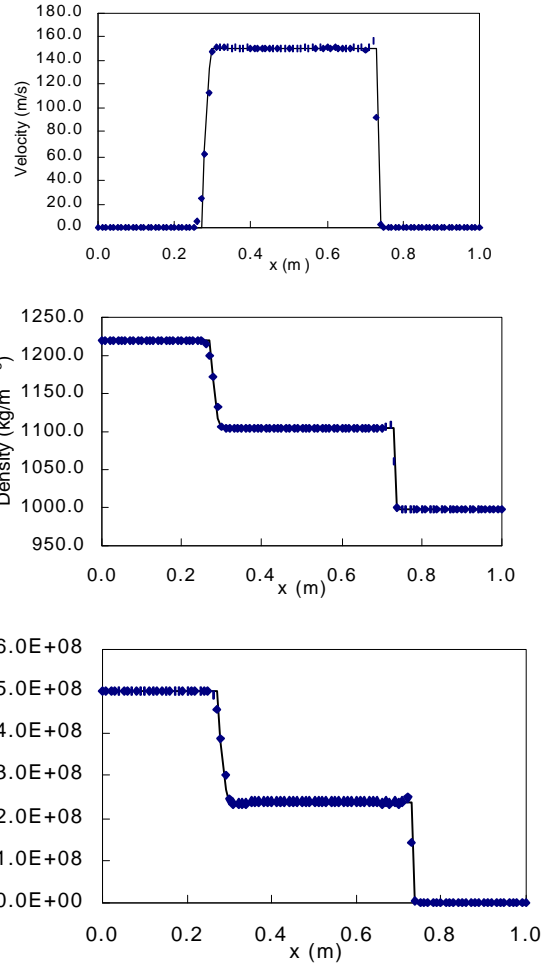


Fig. 3 The CE/SE solution of hydraulic shock problem ($t=0.15 \times 10^{-3}$ sec.)

3.3.2 Cavitating Pipe Flows

In this case, the calculation is initialized by a pipe flow at a steady state. When $t=0$, an upstream valve is suddenly closed. Due to the inertia of the liquid flow, however, the liquid continues to flow in the pipe. Thus, a vacuum region (cavitation) occurs in the neighborhood of the valve. The low pressure of the vacuum region imposes an adverse pressure gradient to the pipe flow, and eventually causes the liquid to flow in a reverse direction back to the valve. The collapse of the cavitation region creates a pressure surge. As a result, fluid flow changes the direction again and flows away from the valve. The back and forth oscillations of the pipe flows is the phenomenon that we want to simulate by using the CE/SE method.

Figure 5 shows the series of the pressure distribution along the pipe with an interval of 0.185 seconds. The horizontal axis represents the pipe and vertical axis represents the pressure head. A logarithmic (base 10) scale is used for the vertical axis from 0.1m to 100m. The arrows in this figure indicate the wave propagation directions. It's interesting to see that wave propagation speed varies considerably during the first 4.5 seconds after the valve closure. This is because the sonic speed of two phase flow is very sensitive to the void fraction of

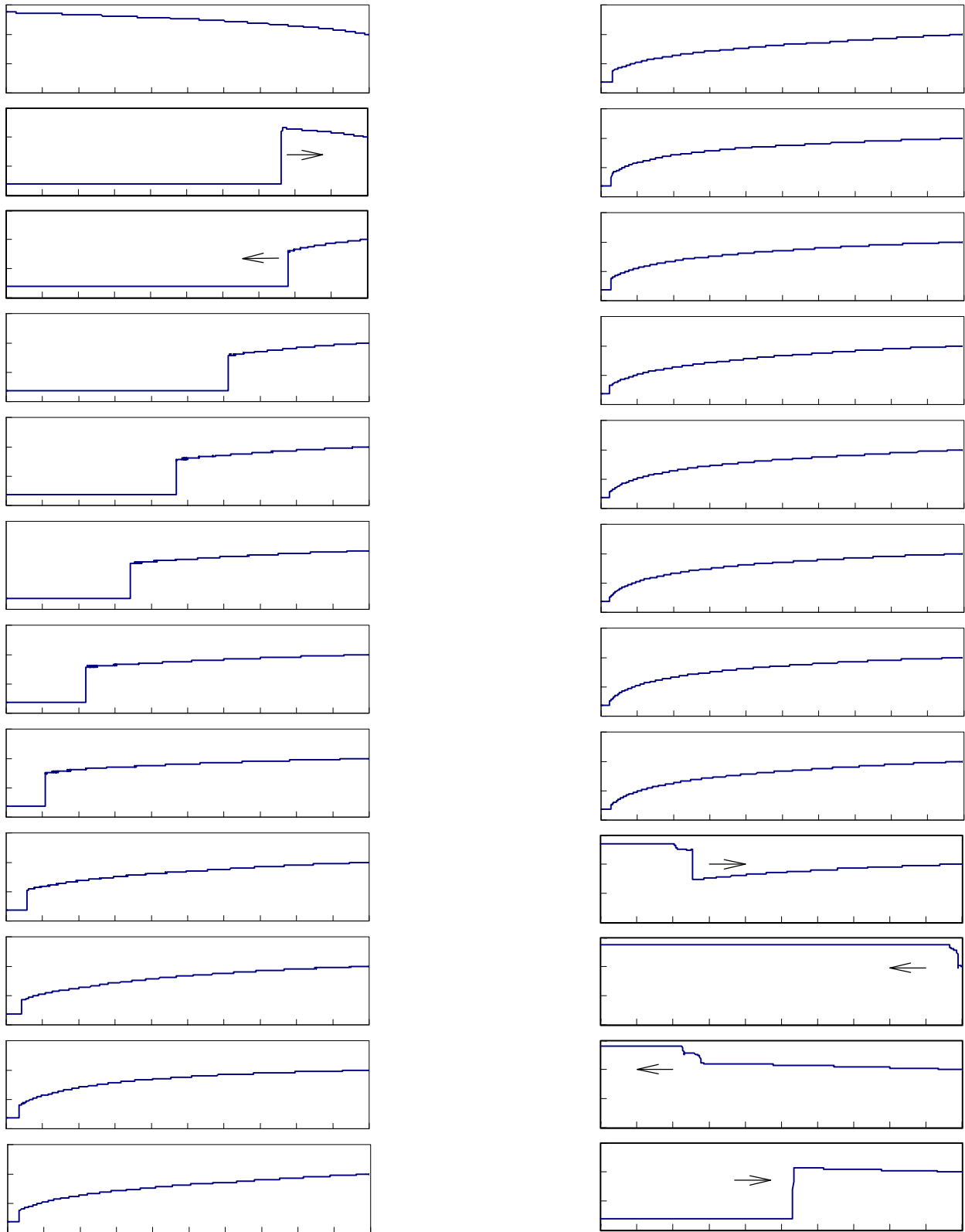


Fig. 5 Series of the pressure distribution along the pipe (interval time = 0.185sec.)

the flow. The sound speed of mixture of water and its vapor can be as low as 20m/s.

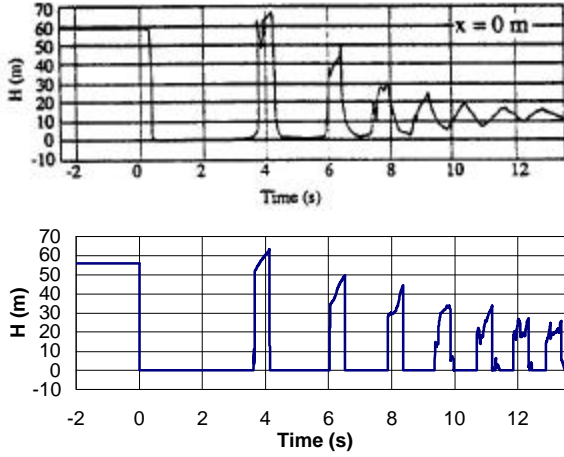


Fig. 6 Cavitation caused by an upstream closing valve: (a) Experimental result, (b) Numerical simulation results.

Figure 6 shows the pressure history on the valve surface with (a) as the experimental data and (b) the numerical results by the CE/SE method. The numerical results compared favorably with the experimental data in terms of the pressure pick and the oscillation period. We remark that in the later stage of the flow development, experimental data showed more damped condition. This is due to fact that the use of a simple one-dimensional viscous model in our model, Eq.(2.2), is inadequate to represent the real mechanism of flow friction, which is by and large caused by the boundary layer effect.

Figure 7 shows the pressure history of a cavitating flow, where the valve is located at the downstream of the pipe. Again, the comparison is very favorable.

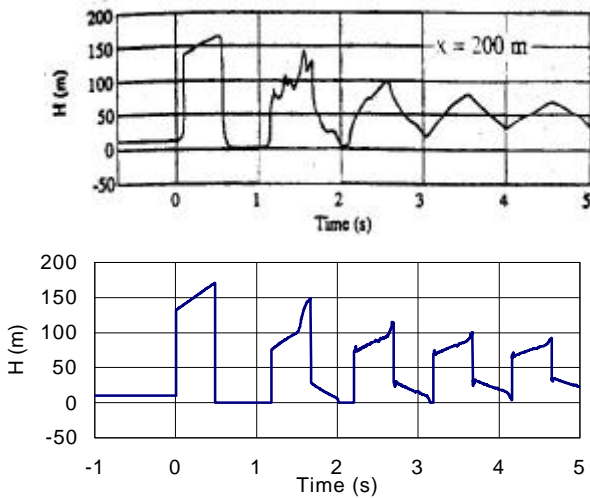


Fig. 7 Cavitation caused by a downstream closing valve: (a) Experimental result, (b) Numerical simulation result.

4. TWO-DIMENSIONAL SIMULATION

4.1 GOVERNING EQUATIONS

The 2D non-dimensionalized governing equation of the two-phase flow is:

$$\frac{\partial \mathbf{U}^*}{\partial t^*} + \frac{\partial \mathbf{E}^*}{\partial x^*} + \frac{\partial \mathbf{F}^*}{\partial y^*} = 0, \quad (4.1)$$

where

$$\mathbf{U}^* = \begin{bmatrix} \mathbf{r}^* \\ \mathbf{r}^* u^* \\ \mathbf{r}^* v^* \end{bmatrix}, \quad \mathbf{E}^* = \begin{bmatrix} \mathbf{r}^* u^* \\ \mathbf{r}^* u^{*2} + p^* - \mathbf{t}_{xx}^* \\ \mathbf{r}^* u^* v^* - \mathbf{t}_{xy}^* \end{bmatrix}$$

$$\mathbf{F}^* = \begin{bmatrix} \mathbf{r}^* v^* \\ \mathbf{r}^* u^* v^* - \mathbf{t}_{xy}^* \\ \mathbf{r}^* v^{*2} + p^* - \mathbf{t}_{yy}^* \end{bmatrix}.$$

The non-dimensionalizing procedure is based on L , V_∞ , ρ_∞ and μ_∞ , where L is the chord length. Here ρ^* is the density of the two-phase flow, which varies between the vapor density and the liquid density. We also employed the homogenous cavitation model stated in section 3 to relate the density to the pressure of the cavitating flows. The Reynolds number Re , pressure coefficient C_p and cavitation number σ are defined as follows:

$$Re = \frac{V_\infty^* L^* \mathbf{r}^*}{\mathbf{m}_\infty^*}, \quad C_p = \frac{(p^* - p_\infty^*)}{0.5 \mathbf{r}^* V_\infty^{*2}}, \quad \mathbf{s} = \frac{(p_\infty^* - p_v^*)}{0.5 \mathbf{r}^* V_\infty^{*2}} \quad (4.2)$$

4.2 SIMULATION RESULTS

The Navier-Stokes solver employed in this paper uses unstructured triangular mesh. Figure 8 shows the calculation mesh around NACA0015 airfoil at zero attach angle.

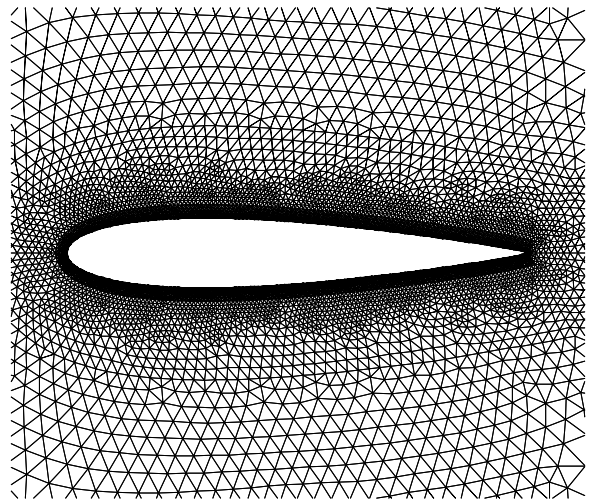


Fig. 8 Unstructured triangular mesh around NACA0015.

Figure 9 shows the void fraction contours under the condition of 20° attach angle and $\sigma = 1.2$. The outside most contour represents void fraction 0.01, where the fluid is almost liquid. The reseat contours are from 0.1 to 1 with an increasement of 0.1. We assume the cavity shape is represented by the contour 0.1, as used by Kubota etc.[14]. This results agree with the experimental results of Kubota etc.[14]. The disgreement at the tail of the cavity is due to the simplicity of the current cavitation model. The homogenous model cannot resolve the shedding bubbles in the down stream of the attached cavity, where the pressure of the flow is higher than the vapor pressure of fluid.

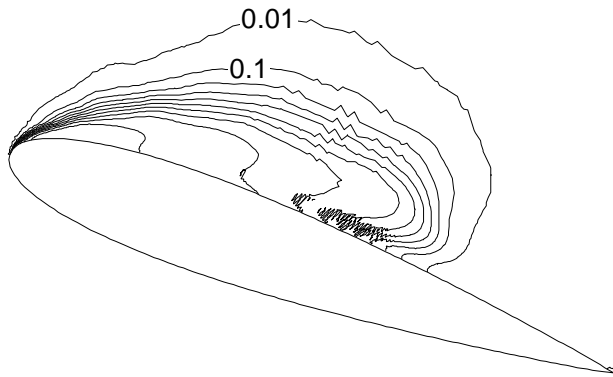


Fig. 9 Void fraction contours around NACA0015. attack angle = 20° , $Re=3 \times 10^5$, $\sigma = 1.2$.

Figure 10 shows the velocity distribution under the condition of 20° attach angle and $\sigma = 1.2$. A strong vortex is formed at the tail of the cavity. The interaction between the vortex and the cavity lead to the re-entrant flow at the tail of the cavity, as shown in Fig. 9. The importance of re-entrant flows was emphasized by Knapp [15], and experimentally and theoretically studied by Furness ad Hutton[16].

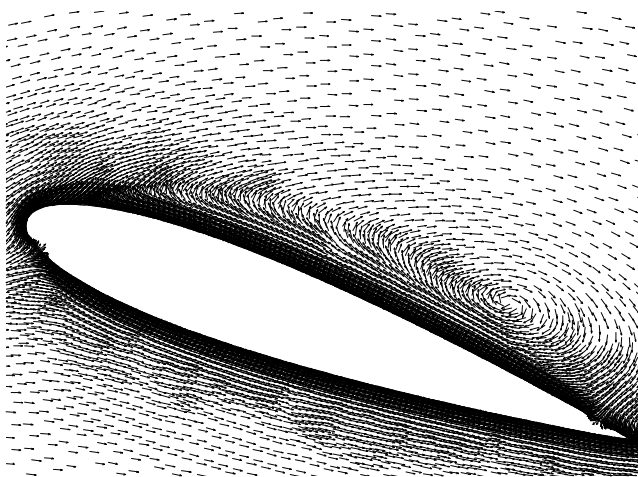


Fig. 10 Velocity distribution around NACA0015. attack angle = 20° , $Re=3 \times 10^5$, $\sigma = 1.2$.

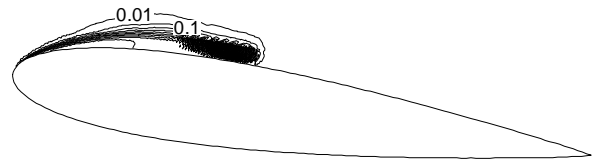


Fig. 11 Void fraction contours around NACA0015. attack angle = 8° , $Re=3 \times 10^5$, $\sigma = 1.2$.

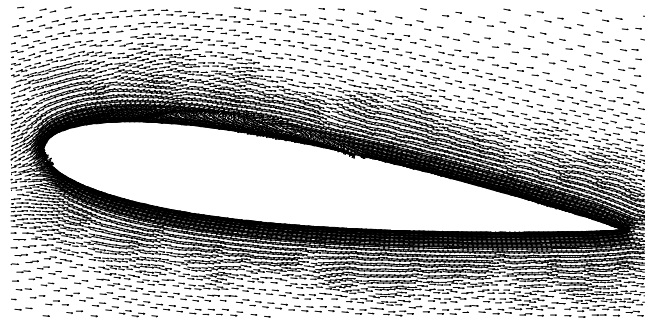


Fig. 12 Velocity distribution around NACA0015. attack angle = 8° , $Re=3 \times 10^5$, $\sigma = 1.2$.

Figure 11 and 12 show the void fraction contours and velocity distribution around NACA0015 under the same conditions except the attack angle is 8 degrees. The cavity shape is much smaller in this case, as shown in Fig. 11. This agrees with Kubota's experimental results. There is also a vortex formed near the upper side of the airfoil, which is much more near the airfoil surface and moved to the head position. But the vortex is still at the tail of the cavity. This indicates the strong interaction between the vortex and cavity.

5. CONCLUDING REMARKS

In this paper, we reported the extension of the CE/SE method to calculate cavitating flows. The CE/SE method is simple, accurate, and very efficient in calculating the complicated flow phenomenon of cavitation. Two examples are reported: (1) one-dimensional internal pipe flows and (2) two-dimensional external flows around NACA0015 airfoil, the CE/SE was capable to capture all salient features of the flow field, and the numerical results compared favorably with the experimental data and analytical solution.

ACKNOWLEDGEMENT

REFERENCES

1. Chang S. C., 1995, "The Method of Space-Time Conservation Element and Solution Element – A New Approach for Solving the Navier-Stokes and Euler

- Equations," *Journal of computational Physics*, Vol. 119, pp. 295-324.
2. Chen Y. and Heister S. D., 1995, "Two-Phase Modeling of Cavitated Flows," *Computers and Fluids*, Vol. 24, No. 7, pp. 799-809.
 3. Li W. H. and Walsh J. P., 1964, "Pressure Generated by Cavitation in a Pipe," *Journal of the Engineering Mechanics Division, Proceedings of the American Society of Civil Engineers*, pp. 113-133.
 4. Marcic M. and Kovacic Z., 1985, "Computer Simulation of the Diesel Fuel Injection System," SAE Paper 851583.
 5. Onorati A. and Ferrari G., 1998, "Modeling of 1-D Unsteady Flows in I.C. Engine Pipe Systems: Numerical Methods and Transport of Chemical Species," SAE Paper 980782.
 6. Ozol J., Kim J. H. and Healzer J., 1994, "Cavitation Experience with Control Valves in Nuclear Power Plants," FED-Vol. 190, *Cavitation and GAS-Liquid Flow in fluid Machinery and Devices*, ASME.
 7. Schmidt D. P., 1997, "Cavitation in Diesel Fuel Injector Nozzles," Ph. D. Thesis.
 8. Shu J. -J., Edge K. A., Burrows C. R., and Xiao S., 1993, "Transmission Line Modelling with Vaporous Cavitation," Presented at the ASME Winter Annual Meeting, 93-WA/FPST-2.
 9. Sobel D. R. and Lehrach R. P. C., 1987, "A Hydro-Mechanical Simulation of Diesel Fuel Injection Systems," SAE Paper 870432.
 10. Strunk R. D., 1991, "The Dynamics of Pump-Line-Nozzle Fuel Injection Systems," SAE Paper 91181.
 11. Tang H. S. and Huang D., 1996, "A Second-Order Accurate Capturing Scheme for 1D Inviscid Flows of Gas and Water with Vacuum Zones," *Journal of Computational Physics*, 128, pp. 301-318.
 12. Wallis G. B., 1969, *One-dimensional Two-phase Flow*, McGraw-Hill Book Company.
 13. Yu S. T. and Chang S. C., 1997, "Treatments of Stiff Source Terms in Conservation Laws by the Method of Space-Time Conservation Element and Solution Element," AIAA 97-0435.
 14. Kubota A., Kato, H. and Yamaguchi H., 1992, "A New Modelling of Cavitating Flows: a Numerical Study of Unsteady Cavitation on a Hydrofoil section," *Journal of Fluids Mechanics*, Vol. 240, pp. 59-96.
 15. Knapp, R.T., 1956, "Further Studies on the Mechanisms and Damage Potential of Fixed Cavities," Paper 19, 1955 Symposium at NPL, HMSO, London.
 16. Furness R. A. and Hutton S.P., 1975, "Experimental and Theoretical Studies of Two-Dimensional Fixed-Type Cavities," *Journal of Fluids Engineering*, December, pp. 515-522.